

# Stabilized Molybdenum Trioxide Nanowires as Novel Ultrahigh-Capacity Cathode for Rechargeable Zinc Ion Battery

Xinjun He, Haozhe Zhang, Xingyu Zhao, Peng Zhang, Minghua Chen,\* Zhikun Zheng, Zhiji Han, Tingshun Zhu, Yexiang Tong, and Xihong Lu\*

Exploration of high-performance cathode materials for rechargeable aqueous Zn ion batteries (ZIBs) is highly desirable. The potential of molybdenum trioxide (MoO<sub>3</sub>) in other electrochemical energy storage devices has been revealed but held understudied in ZIBs. Herein, a demonstration of orthorhombic MoO<sub>3</sub> as an ultrahigh-capacity cathode material in ZIBs is presented. The energy storage mechanism of the MoO<sub>3</sub> nanowires based on Zn<sup>2+</sup> intercalation/deintercalation and its electrochemical instability mechanism are particularly investigated and elucidated. The severe capacity decay of the MoO<sub>3</sub> nanowires during charging/discharging cycles arises from the dissolution and the structural collapse of MoO<sub>3</sub> in aqueous electrolyte. To this end, an effective strategy to stabilize MoO<sub>3</sub> nanowires by using a quasi-solid-state poly(vinyl alcohol)(PVA)/ZnCl<sub>2</sub> gel electrolyte to replace the aqueous electrolyte is developed. The capacity retention of the assembled ZIBs after 400 charge/discharge cycles at 6.0 A g<sup>-1</sup> is significantly boosted, from 27.1% (in aqueous electrolyte) to 70.4% (in gel electrolyte). More remarkably, the stabilized quasi-solid-state ZIBs achieve an attracting areal capacity of 2.65 mAh cm<sup>-2</sup> and a gravimetric capacity of 241.3 mAh g<sup>-1</sup> at 0.4 A g<sup>-1</sup>, outperforming most of recently reported ZIBs.


## 1. Introduction

With the fast-growing demand in energy-consuming products like electric vehicles and portable electronics, it is imperative to explore advanced energy storage technologies with high energy, good safety, and affordable cost.<sup>[1–8]</sup> As one of the most promising energy storage devices, aqueous zinc-ion batteries (ZIBs) has gained ever-increasing attention on account of its outstanding safety, high theoretical capacity (Zn: ≈820 mAh g<sup>-1</sup>), low cost as well as environmental benignity.<sup>[9–15]</sup> In addition, the aqueous ambient of the electrodes also accelerates the ion diffusion owing to the high ionic conductivity, which enables them a better rate capability.<sup>[16–18]</sup> Despite these advanced features, one of the biggest block for ZIBs developed to date is their relatively low capacity in terms of the substantially inferior capacity of cathode materials

than Zn anode.<sup>[19–21]</sup> To this end, numerous research efforts have been focused on the exploiting of high-capacity cathode materials over the past few decades.<sup>[21–24]</sup> A great variety of materials including MnO<sub>2</sub>,<sup>[25–28]</sup> ZnMn<sub>2</sub>O<sub>4</sub>,<sup>[17]</sup> Zn<sub>x</sub>Mo<sub>6</sub>S<sub>6</sub>,<sup>[29]</sup> ZnHCF,<sup>[30]</sup> Zn<sub>0.25</sub>V<sub>2</sub>O<sub>5</sub>·nH<sub>2</sub>O,<sup>[31]</sup> VS<sub>2</sub>,<sup>[20]</sup> NiOOH,<sup>[32]</sup> and Co<sub>3</sub>O<sub>4</sub><sup>[9]</sup> have been reported as promising cathodes with good electrochemical performance. For example, Wu and co-workers employed ultrathin porous Co<sub>3</sub>O<sub>4</sub> nanosheets which was electrodeposited on Ni foam as a cathode material, and it delivered a capacity of 0.32 mAh cm<sup>-2</sup> in Zn//Co<sub>3</sub>O<sub>4</sub> battery (0.05 A g<sup>-1</sup>).<sup>[9]</sup> Pan and co-workers used a hydrothermal method to synthesize α-MnO<sub>2</sub> nanofibers, which exhibited a capacity of 1.43 mAh cm<sup>-2</sup> at 0.1 A g<sup>-1</sup>.<sup>[33]</sup> Nevertheless, the capacity of reported ZIBs is still unsatisfactory for future high-energy electronics. Developing new cathode materials with high capacity and excellent durability are yet challenging and highly desirable.

Orthorhombic MoO<sub>3</sub> nanomaterials serve as versatile electrodes for Li ion battery and supercapacitors because of their multiple valence states and unique layered structures.<sup>[13,34–37]</sup> In previous studies, MoO<sub>3</sub> has shown its reversible Li-ion insertion/extraction ability.<sup>[36,37]</sup> Given that the similar ion radius of Zn<sup>2+</sup> (0.75 Å) and Li<sup>+</sup> (0.76 Å), it is expected that the MoO<sub>3</sub> holds great promise as high-performance electrode for ZIBs.<sup>[9,26]</sup> However, to our knowledge, there are few reports

X. He, X. Zhao, Prof. M. Chen, Prof. X. Lu  
Key Laboratory of Engineering Dielectric and Applications  
(Ministry of Education)  
Harbin University of Science and Technology  
Harbin 150080, China  
E-mail: mhchen@hrbust.edu.cn; luxh6@mail.sysu.edu.cn  
X. He, H. Zhang, Prof. Z. Zheng, Prof. Z. Han, Prof. T. Zhu,  
Prof. Y. Tong, Prof. X. Lu  
MOE of the Key Laboratory of Bioinorganic and Synthetic Chemistry  
The Key Lab of Low-Carbon Chem & Energy Conservation  
of Guangdong Province  
School of Chemistry  
Sun Yat-Sen University  
Guangzhou 510275, P. R. China  
Dr. P. Zhang  
School of Environment and Civil Engineering  
Guangdong Engineering and Technology Research Center  
for Advanced Nanomaterials  
Dongguan University of Technology  
Dongguan 523808, China

 The ORCID identification number(s) for the author(s) of this article can be found under <https://doi.org/10.1002/advs.201900151>.

© 2019 The Authors. Published by WILEY-VCH Verlag GmbH & Co. KGaA, Weinheim. This is an open access article under the terms of the Creative Commons Attribution License, which permits use, distribution and reproduction in any medium, provided the original work is properly cited.

DOI: 10.1002/advs.201900151

on the exploration of molybdenum oxides as electrode in ZIBs. In this work, we first investigated the electrochemical properties of orthorhombic MoO<sub>3</sub> nanowires as Zn<sup>2+</sup> storage electrode and demonstrated their implementation as high-capacity cathode in ZIBs. The energy storage behavior of the orthorhombic MoO<sub>3</sub> based on Zn<sup>2+</sup> intercalation/deintercalation mechanism as well as its unstable mechanism were systematically unraveled by comprehensive characterizations. More importantly, an effective approach of using a quasisolid state electrolyte to stabilize MoO<sub>3</sub> nanowires was developed. Electrochemical studies revealed that the ZIBs based on our MoO<sub>3</sub> nanowire cathode in a quasisolid state poly(vinyl alcohol)(PVA)/ZnCl<sub>2</sub> gel electrolyte achieve an ultrahigh capacity of 2.65 mAh cm<sup>-2</sup> (243.1 mAh g<sup>-1</sup>) at 0.4 A g<sup>-1</sup> and an impressive energy density of 14.4 mWh cm<sup>-3</sup>. Additionally, the cycling stability of this quasisolid state ZIB device is significantly improved compared to the device with aqueous electrolyte, maintaining more than 70.4% of its initial capacity after 400 cycles.

## 2. Results and Discussion

MoO<sub>3</sub> nanowires were synthesized through a quick and facile seed-assisted hydrothermal method (details in Experimental Section). To characterize the morphology of the as-synthesized nanowire, scanning electron microscopy (SEM) and transmission electron microscopy (TEM) were carried out. As shown in **Figure 1a**, MoO<sub>3</sub> nanowires with a diameter of about 100 nm are vertically grown on fibers of carbon cloth, and these nanowires intertwine to form bundles. **Figure 1b** displays the typical TEM image of the MoO<sub>3</sub> nanowires, presenting its wire-like morphology. The diameter of the nanowire is around 100 nm, which is well in agreement with SEM observation. Lattice fringes are observed in the high resolution TEM (HRTEM) image (**Figure 1c**), showing the polycrystalline nature of these MoO<sub>3</sub> nanowires. This is

further validated by the bright diffraction spots of its corresponding selected area electron diffraction (SAED) pattern (**Figure 1c**, inset). The lattice fringe with a *d*-spacing of about 0.38 nm is attributed to (110) plane of orthorhombic MoO<sub>3</sub> (JCPDS#76-1003).

To explore the crystal structure and valance state of Mo, we conducted powder X-ray diffraction (XRD) and X-ray photoelectron spectroscopy (XPS) measurements. The representative XRD pattern of the MoO<sub>3</sub> sample is collected in **Figure 1d**. All of the diffraction peaks can be well assigned to orthorhombic MoO<sub>3</sub> (JCPDS#76-1003) with space group of Pbnm(62), indicating the as-obtained product is highly pure. The corresponding crystalline structure is shown in **Figure 1e**. [MoO<sub>6</sub>] octahedra share edges in *c*-direction and are linked by corners in *a*-direction to construct a layer in *ac*-plane.<sup>[36,37]</sup> Then, these parallel layers stack through van der Waals force along *b*-direction to form MoO<sub>3</sub> layer architecture. It is believed that such unique layered structure is highly favorable for ion intercalation/deintercalation. **Figure S1** of the Supporting Information presents the XPS survey spectrum of the MoO<sub>3</sub> sample. Only three elements (Mo, O, and C) are detected on the surface of MoO<sub>3</sub> sample, further indicating the high purity of these nanowires. The core-level Mo 3d XPS spectrum can be deconvoluted into two peaks, as shown in **Figure 1f**. The peaks at the binding energy of 233.36 and 236.51 eV are the characteristic Mo 3d<sub>5/2</sub> and 3d<sub>3/2</sub> peaks of Mo<sup>6+</sup>.<sup>[38]</sup> In addition, the ratio of Mo and O atom% obtained from XPS result is about 1:3 (inset in **Figure 1f**). All these findings adequately support that the as-synthesized product is polycrystalline orthorhombic MoO<sub>3</sub> nanowires.

An aqueous ZIB device was assembled to evaluate the electrochemical properties of the as-obtained MoO<sub>3</sub> nanowires, with a commercial zinc plate as anode and aqueous 2 M ZnCl<sub>2</sub> solution as electrolyte (named as Zn//MoO<sub>3</sub> battery). **Figure 2a** presents the typical cyclic voltammetry (CV) curve of this MoO<sub>3</sub> nanowires at a scan rate of 1 mV s<sup>-1</sup>. A couple of well-defined redox peaks at around 0.85 and

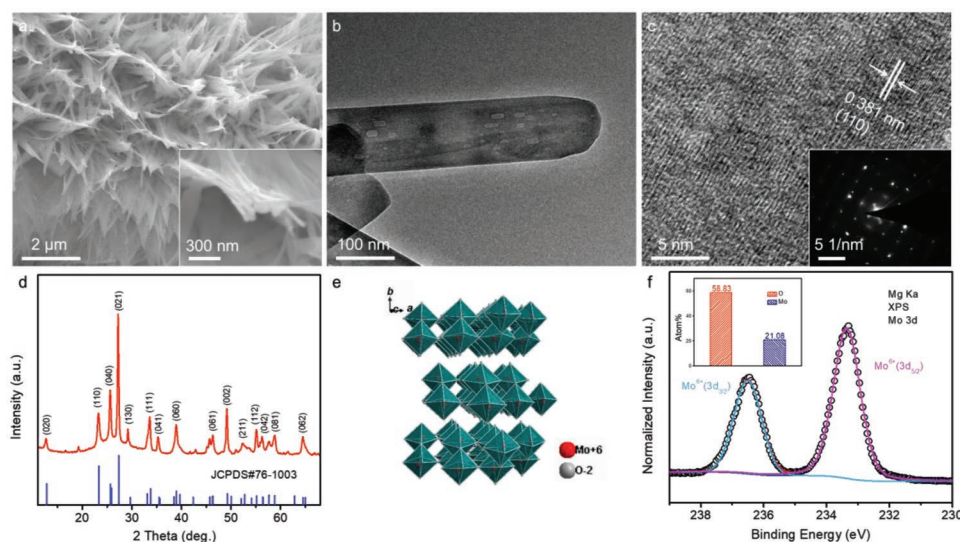


**Figure 1.** a) SEM images, b) TEM image, c) HRTEM image, d) XRD pattern, e) layered crystal structure, and f) core-level Mo 3d of XPS spectrum of the MoO<sub>3</sub> nanowires. The insets in (c,f) are its corresponding SAED pattern and the atom% of Mo and O, respectively.

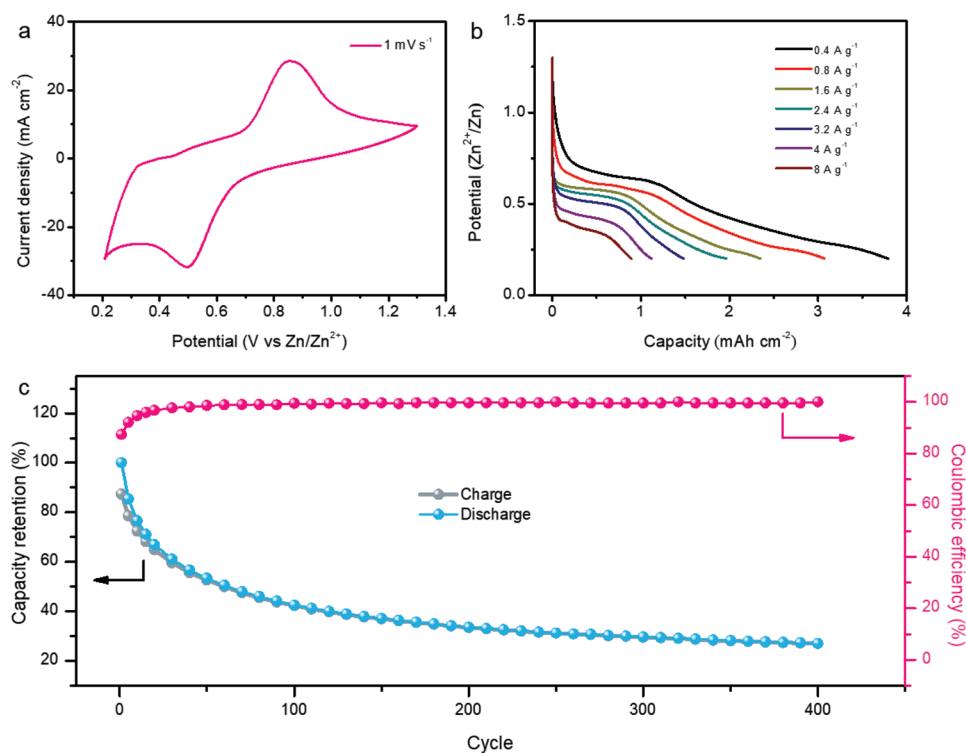


**Figure 2.** a) CV curves of the aqueous Zn//MoO<sub>3</sub> battery in 2M ZnCl<sub>2</sub> electrolyte at 1 mV s<sup>-1</sup>. b) Galvanostatic charge and discharge curves of Zn//MoO<sub>3</sub> battery at different current densities. c) Lifespan of the aqueous device at current density of 6.0 A g<sup>-1</sup>.

0.50 V versus Zn<sup>2+</sup>/Zn is clearly identified, which shows an evident battery behavior. The obvious plateaus in galvanostatic charge–discharge curves collected at different current densities also identify the redox reactions (Figure 2b). Additionally, the calculated areal capacity of this Zn//MoO<sub>3</sub> battery reaches 3.79 mAh cm<sup>-2</sup> (344.8 mAh g<sup>-1</sup> based on the mass of the MoO<sub>3</sub>), substantially larger than most of the developed ZIBs.<sup>[9,17,20,33]</sup> However, this Zn//MoO<sub>3</sub> battery is found to suffer from severe capacity loss. As given by Figure 2c, its capacity declines rapidly in the first several cycles and only 27.1% of the initial capacity is preserved after 400 charge–discharge cycles, which makes it to be far away from practical application.

To elucidate the mechanism and the origin of the instability of the Zn//MoO<sub>3</sub> battery, the component and structural evolution of the orthorhombic MoO<sub>3</sub> cathode during the charge–discharge process were meticulously investigated by the ex-situ XRD, XPS, TEM-energy dispersive X-ray spectroscopy (TEM-EDX) and UV–Visible spectroscopy analyses. XRD test was conducted under different voltages in the first and second charge–discharge cycles. In the first discharging segment, the set of (0*k*0) reflections including (020), (040), and (060), obviously shift toward lower positions when the voltage decreases from 0.64 to 0.50 V (Figure S2, Supporting Information). This fact suggests the expansion of the interlayer spacing due to the Zn<sup>2+</sup> intercalation. As the voltage further decreases to 0.2 V, the continuous expansion of (020) interplanar spacing is observed whereas (040) and (060) reflections vanish gradually. According to the Bragg equation, the interlayer distance of (020) is calculated to increase from 6.9 to

7.3 Å during the whole discharging process. Moreover, the disappearance of (040) and (021) peaks indicates that Zn<sup>2+</sup> not only inserts into the empty sites of the inter layer (ac plane) but also exists between the adjacent MoO<sub>6</sub> octahedrons.<sup>[39,40]</sup> In the second charge/discharge cycle, all of the peaks in XRD pattern show invertible shift during charge/discharge process (Figure 3a). For example, the peak at 46.2° in region 2 shifts to 47.1° when the voltage increases from 0.2 to 1.3 V, which suggests the shrink of the MoO<sub>3</sub> lattice. This can be ascribed to different Zn<sup>2+</sup>/vacancy ordering patterns when the Zn<sup>2+</sup> inserts into and extracts from the cathode.<sup>[31]</sup> Additionally, after this charging process, the XRD pattern has not recovered from discharged state to original state, which indicates that a part of inserted Zn<sup>2+</sup> remained in the MoO<sub>3</sub> lattice. More XRD patterns of extraction-state MoO<sub>3</sub> during cycling have been collected in Figure S3 (Supporting Information). It can be seen that the pattern of first cycle has changed a lot compared with initial MoO<sub>3</sub> and gradually become stabilized in subsequent cycles, suggesting the formation of solid electrolyte interface (SEI) layer at the initial cycles.<sup>[36,37]</sup> Simultaneously, Figure S4 of the Supporting Information shows that the zinc content of the extraction-state MoO<sub>3</sub> keeps increasing in the first four cycles, which confirms the above conclusion and it also explains the slightly lower Coulombic efficiency for the first several charge/discharge cycles.

Figure 3b compares the core levels Mo 3d XPS spectra of the MoO<sub>3</sub> nanowires under insertion (0.2 V) and extraction (1.3 V) states. At 0.2 V, the exclusive existence of Mo<sup>4+</sup> (3*d*<sub>3/2</sub>: 235.82 eV), Mo<sup>5+</sup> (3*d*<sub>3/2</sub>: 234.77 eV), and Mo<sup>6+</sup> (3*d*<sub>3/2</sub>: 233.67 eV) evidently shows its deep discharging nature.<sup>[38,41]</sup>

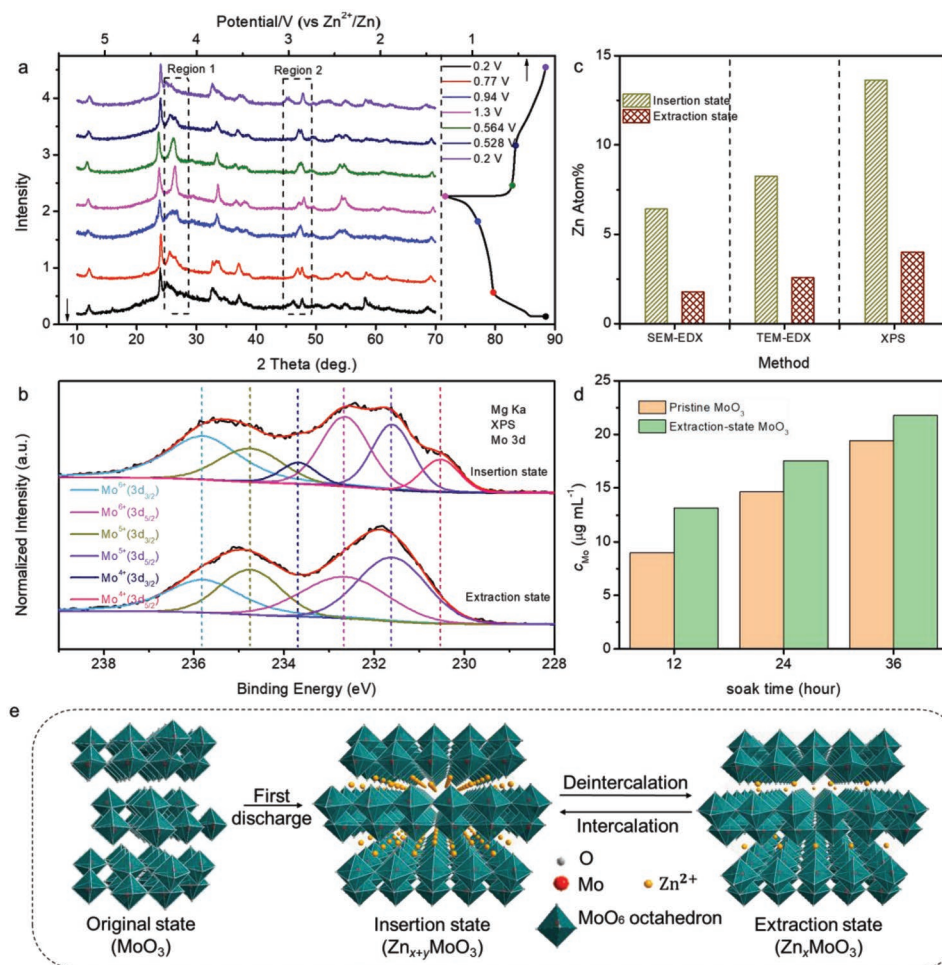
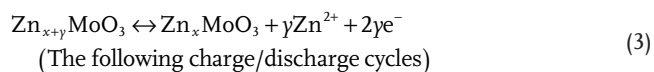
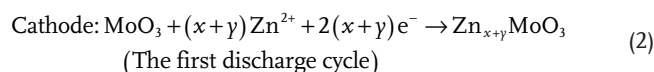


**Figure 3.** a) XRD pattern of MoO<sub>3</sub> at different voltage. b) Core-level Mo 3d XPS spectra and c) Zn Atom% obtained by different methods of MoO<sub>3</sub> nanowires in insertion (0.2 V) and extraction (1.3 V) state. d) C<sub>Zn</sub> for aqueous electrolyte after pristine MoO<sub>3</sub> and extraction-state MoO<sub>3</sub> were immersed for different time. e) Schematic illustration of the Zn<sup>2+</sup> intercalation/deintercalation mechanism for orthorhombic MoO<sub>3</sub> electrode.

When the voltage is applied to 1.3 V, the Mo<sup>4+</sup> peaks fades away, indicating the Mo<sup>4+</sup> gradually turns to its higher valence state (Mo<sup>6+</sup> and Mo<sup>5+</sup>) with Zn<sup>2+</sup> constantly extracts out from the framework. The existence of Mo<sup>5+</sup> in the extraction state indicates that Zn<sup>2+</sup> has not totally deintercalated from MoO<sub>3</sub> framework. Core-level Zn 3p XPS spectrum of electrode in pristine, insertion, and extraction state were given in Figure S5 (Supporting Information). Upon discharging, a substantial leap of Zn 2p (2p<sub>3/2</sub>: 1022.2 eV) signal is recorded, which confirms the Zn<sup>2+</sup> intercalation and deintercalation mechanism. Similarly, Figure 3c shows the Zn atom% of insertion state (0.2 V) and extraction state (1.3 V) obtained by three different methods, again revealing the intercalation and deintercalation of Zn<sup>2+</sup> ions. All of these methods presented that Zn atom% of the insertion state in MoO<sub>3</sub> nanowires is more than twice as much as that of the extraction state. Combined with TEM-Mapping images (Figure S6, Supporting Information) where Zn<sup>2+</sup> is homogeneously distributed in the insertion/extraction sample, it is deduced that Zn<sup>2+</sup> uniformly intercalates into the whole MoO<sub>3</sub> cathode upon discharging. Meanwhile, the existence

of zinc signal in extraction-state MoO<sub>3</sub> also suggests that Zn<sup>2+</sup> has not completely extracted from the cathode, which is well consistent with XRD and other characterizations. Based on the above results, the overall reactions of our Zn//MoO<sub>3</sub> battery can be summarized as



SEM and UV-Visible spectroscopy were carried out to probe into the poor cycling stability of MoO<sub>3</sub> cathode in aqueous electrolyte. SEM and element mapping (Figure S7, Supporting Information) was operated on MoO<sub>3</sub> under insertion and extraction states. In extraction state, the wire morphology

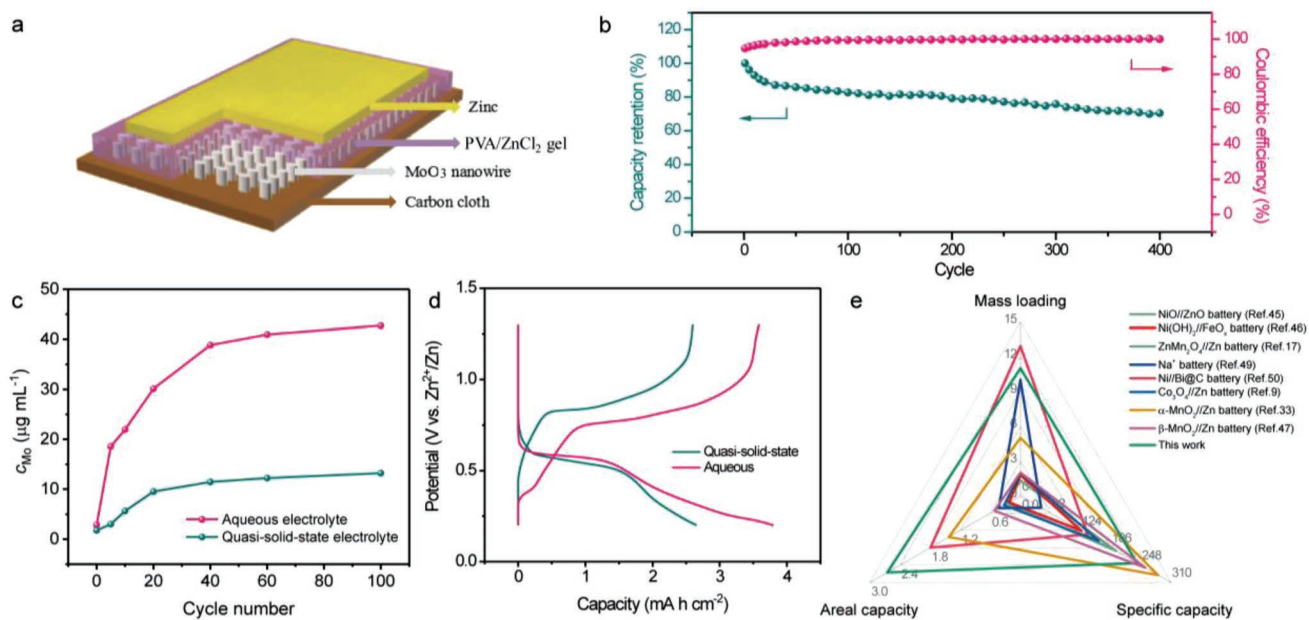


**Figure 4.** a) Schematic illustration of the quasisolid state Zn//MoO<sub>3</sub> battery. b) Cycling performance of the quasisolid state Zn//MoO<sub>3</sub> battery at a current density of 6.0 A g<sup>-1</sup>. c) Calculated C<sub>Mo</sub> for aqueous and quasisolid state electrolyte after different cycles. d) Charge/discharge curves of the aqueous and quasisolid state Zn//MoO<sub>3</sub> batteries at current density of 0.4 A g<sup>-1</sup>. e) The capacities of the quasisolid state Zn//MoO<sub>3</sub> battery and some recently reported works.<sup>[9,17,33,45–47,49,50]</sup>

with a diameter of around 100 nm is well retained. However, after Zn<sup>2+</sup> insertion, a sheet-like structure with a thickness of 100 nm is captured. Combining with the corresponding element mapping data, we observed that the extraction state MoO<sub>3</sub> has much lower Zn element ratio than insertion state, which is also consistent with the XRD and TEM mapping results. To further uncover the morphology change phenomenon, we have conducted ex-situ SEM to test samples in different voltages (corresponding to different Zn<sup>2+</sup> intercalation ratio) in one charge–discharge cycles. As shown in Figure S8 of the Supporting Information, when the electrode charged to 0.77 V where starts the charging plateau, a sheet morphology is presented. With the deintercalation of Zn<sup>2+</sup>, those sheets gradually separate and finally change back to nanowires (at 0.94 V and finally to 1.3 V). On the contrary, with the processing of intercalation of Zn<sup>2+</sup>, the nanowires slowly aggregate to form bundles and finally become nanosheets in the insertion-state MoO<sub>3</sub>. Moreover, the sheet morphology also occurs during charge and discharge between 4 and 0.4 A g<sup>-1</sup> current density (Figure S9, Supporting Information), and it is more obvious at low current density, which may because more Zn<sup>2+</sup> insert into MoO<sub>3</sub> at a low current density and thus leads to a bigger morphology change. Indeed, the detailed morphology transformation mechanism is still unclear, and relative work is ongoing.

The concentration of Mo species in electrolyte (C<sub>Mo</sub>) was also recorded by UV–Visible spectroscopy to investigate the dissolution situation of the active material. The standard curve of Mo concentration was provided in Figure S10 (Supporting Information). Figure 3d compares the C<sub>Mo</sub> of aqueous electrolyte after pristine and extraction-state MoO<sub>3</sub> cathodes were soaked for different periods of time (Spectra given in Figure S11 of the Supporting Information). It shows that the corresponding

C<sub>Mo</sub> of extraction-state MoO<sub>3</sub> is obviously higher than pristine MoO<sub>3</sub>. For example, the C<sub>Mo</sub> values for pristine and extraction-state MoO<sub>3</sub> after 36 h are 19.39 and 21.76 μg mL<sup>-1</sup>, respectively. These results imply that MoO<sub>3</sub> will be spontaneously dissolved in water even without applying a voltage, and the electrode with Zn<sup>2+</sup> existence becomes more vulnerable to water. In this regard, one way to improve the cycling performance of the device is to suppress the severe dissolution of the cathode.

Based on the above analyses, the aqueous electrolyte was replaced by a quasisolid state polyvinyl alcohol (PVA)/ZnCl<sub>2</sub> based electrolyte to improve the stability of the MoO<sub>3</sub> cathode. To demonstrate our hypothesis, a quasisolid state Zn//MoO<sub>3</sub> battery was fabricated, and the schematic diagram of this battery is illustrated in Figure 4a. The electrochemical durability of this quasisolid state Zn//MoO<sub>3</sub> battery was probed by galvanostatic charge–discharge measurement at 6.0 A g<sup>-1</sup> (Figure 4b). As expected, benefitting from the substantially lower water content and slower ion diffusion, this quasisolid state Zn//MoO<sub>3</sub> battery yields remarkably enhanced stability compared to the aqueous Zn//MoO<sub>3</sub> battery. Specifically, it is able to keep more than 70.4% of its original capacity after 400 cycles, dramatically higher than the aqueous one (27.1%) and comparable to the recently reported Zn ion batteries. Meanwhile, compared to aqueous device, the Coulombic efficiency of the Zn//MoO<sub>3</sub> battery at the initial few cycles is also greatly improved in quasisolid state electrolyte (Figures 2c and 4b), suggesting its electrochemical reaction is more reversible. In addition, the C<sub>Mo</sub> of aqueous and quasisolid state electrolytes after different charge/discharge cycles were also monitored when the MoO<sub>3</sub> cathodes were applied to fabricate devices. Figure S12 of the Supporting Information presents the UV–Visible spectra of two kinds of electrolytes after different charge/discharge cycles,

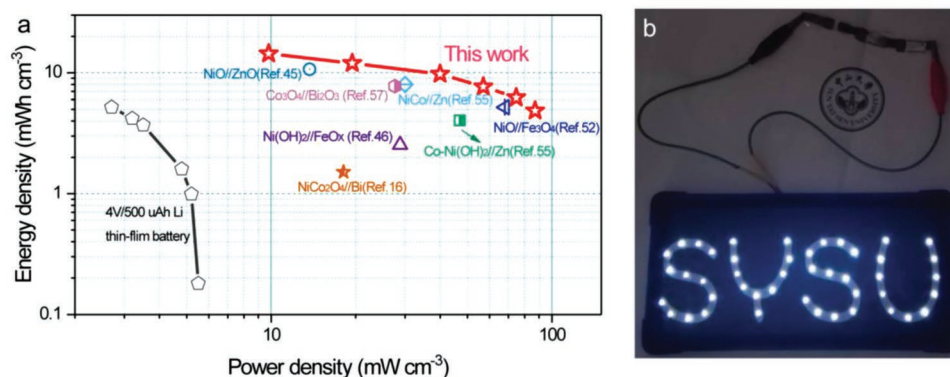


**Figure 5.** a) Ragone plots of quasisolid state Zn//MoO<sub>3</sub> battery with the comparison of other reported electrochemical storage devices.<sup>[16,45,46,51,52,55,57]</sup> b) Picture displays the LED lamps powered by quasisolid state Zn//MoO<sub>3</sub> batteries.

while the corresponding calculated the  $C_{Mo}$  values are shown in Figure 4c. For both electrolyte, the Mo concentration keeps increasing with the proceeding of charging and discharging. After 100 cycles, the detected  $C_{Mo}$  of aqueous electrolyte is  $42.73 \mu\text{g mL}^{-1}$ , which indicates that the dynamic charge/discharge behavior vastly accelerates the dissolution of MoO<sub>3</sub>. More importantly, the  $C_{Mo}$  values of the quasisolid state electrolyte are significantly lower than those of the aqueous electrolyte. For instance, after 100 cycles, the  $C_{Mo}$  in quasisolid state electrolyte is only  $13.22 \mu\text{g mL}^{-1}$ , much smaller than  $42.73 \mu\text{g mL}^{-1}$  of the aqueous electrolyte. The significantly decreased Mo concentration verifying the important role of quasisolid state electrolyte in alleviating the dissolution of MoO<sub>3</sub> and improving the cycling stability of MoO<sub>3</sub> cathode.

Figure 4d compares the charge–discharge curves of the aqueous and quasisolid state Zn//MoO<sub>3</sub> battery at a current density of  $0.4 \text{ A g}^{-1}$ . A couple of charge and discharge plateaus at around 0.82/0.59 V are clearly captured for both devices with aqueous or quasisolid state electrolyte, which suggests that their energy storage mechanisms are similar. This conclusion is also supported by Figure S13 of the Supporting Information, a similar sheet morphology is also characterized after Zn<sup>2+</sup> insertion in quasisolid state electrolyte. Moreover, the Zn atom content in MoO<sub>3</sub> electrode using quasisolid state electrolyte had been measured by XPS in Figure S14 (Supporting Information). It is found that the zinc atom content shows an invertible change from 5.1% to 2.0% and finally to 6.4% at 0.2 V, 1.3 V, and back to 0.2 V, respectively. This dynamic change also confirms its Zn<sup>2+</sup> intercalation–deintercalation mechanism. Compared to aqueous device, the capacity of quasisolid state device shows a visible drop, which can be ascribed to the slower ion diffusion of the quasisolid state battery. To confirm it, the Nyquist plots of the aqueous and quasisolid state Zn//MoO<sub>3</sub> batteries are collected in Figure S15 (Supporting Information). Both of them contain two parts: the high-frequency semicircular loop and the low-frequency straight line, which are relative to charge transfer and ion diffusion, respectively. They are well fitted with the equivalent circuit that inserted in Figure S15 of the Supporting Information, where  $R_{ct}$  means the charge transfer resistance,  $Z_w$  represents the Warburg impedance while CPE is the constant phase element and  $R_e$  is the total ohmic resistance.<sup>[9,42,43]</sup> In comparison with the aqueous Zn//MoO<sub>3</sub> battery, the quasisolid state one exhibits

much lower steep slope in the Warburg region, clearly showing that the ion diffusion rate in quasisolid state electrolyte become much slower. Additionally, the  $R_{ct}$  value of the battery in quasisolid state electrolyte is  $61.2 \Omega$ , which is just slightly larger than  $57.9 \Omega$  for aqueous electrolyte. It suggests that the electrolyte substitution has negligible effect on the electron transportation rate for the electrode. Despite a visible drop of capacity, this quasisolid state battery still delivers impressive capacities of  $2.65 \text{ mAh cm}^{-2}$  and  $241.3 \text{ mAh g}^{-1}$ , which are considerably surpassing most of the recently developed ZIBs and other aqueous batteries (Figure 4e),<sup>[9,17,33,44–50]</sup> such as Ni(OH)<sub>2</sub>//FeO<sub>x</sub> battery ( $0.227 \text{ mAh cm}^{-2}$  and  $126 \text{ mAh g}^{-1}$  at  $1.5 \text{ A g}^{-1}$ ),<sup>[46]</sup> NiO//ZnO battery ( $0.26 \text{ mAh cm}^{-2}$  and  $197.9 \text{ mAh g}^{-1}$  at  $0.38 \text{ A g}^{-1}$ ),<sup>[45]</sup> Zn//Co<sub>3</sub>O<sub>4</sub> battery ( $0.324 \text{ mAh cm}^{-2}$  and  $162 \text{ mAh g}^{-1}$  at  $1 \text{ A g}^{-1}$ ),<sup>[9]</sup> Zn//ZnMn<sub>2</sub>O<sub>4</sub> battery ( $0.3 \text{ mAh cm}^{-2}$  and  $150 \text{ mAh g}^{-1}$  at  $0.05 \text{ A g}^{-1}$ ),<sup>[17]</sup> Zn//β-MnO<sub>2</sub> battery ( $0.516 \text{ mAh cm}^{-2}$  and  $258 \text{ mAh g}^{-1}$  at  $0.2 \text{ A g}^{-1}$ ),<sup>[47]</sup> Zn//α-MnO<sub>2</sub> battery ( $1.425 \text{ mAh cm}^{-2}$  and  $285 \text{ mAh g}^{-1}$  at  $0.1 \text{ A g}^{-1}$ ),<sup>[33]</sup> Na<sup>+</sup> battery ( $0.43 \text{ mAh cm}^{-2}$  and  $43 \text{ mAh g}^{-1}$  at  $0.1 \text{ A g}^{-1}$ ),<sup>[49]</sup> and Ni//Bi@C battery ( $1.79 \text{ mAh cm}^{-2}$  and  $139 \text{ mAh g}^{-1}$  at  $0.31 \text{ A g}^{-1}$ ).<sup>[50]</sup> Particularly, the mass loading of the MoO<sub>3</sub> nanowires is up to  $11.1 \text{ mg cm}^{-2}$ . Such high specific capacity achieved by this MoO<sub>3</sub> electrode also reflects its prominent electrochemical performance. In addition, a high capacity retention of 38.1% ( $1.01 \text{ mAh cm}^{-2}$ ) is exhibited when the current density is increased to  $4 \text{ A g}^{-1}$ , suggesting its excellent performance (Figure S16, Supporting Information). Moreover, the rate performance shows quite similar behavior after being replaced by an aqueous electrolyte with quasisolid state electrolyte (Figure S16, Supporting Information).

Ragone plots in Figure 5a compares the volumetric energy densities and power densities of our quasisolid state Zn//MoO<sub>3</sub> battery with other published aqueous batteries and asymmetric supercapacitors (ASCs). Profiting by the high capacity, the as-fabricated quasisolid state Zn//MoO<sub>3</sub> battery at a power density of  $9.79 \text{ mW cm}^{-3}$  can afford a maximum energy density of  $14.4 \text{ mWh cm}^{-3}$ , which greatly exceeds the value of previously developed aqueous batteries,<sup>[16,44–46,51–56]</sup> including Ni(OH)<sub>2</sub>//FeO<sub>x</sub> ( $2.54 \text{ mWh cm}^{-3}$ ),<sup>[46]</sup> NiCo<sub>2</sub>O<sub>4</sub>//Bi battery ( $1.51 \text{ mWh cm}^{-3}$ ),<sup>[16]</sup> Zn//Co-Ni(OH)<sub>2</sub> ( $4.05 \text{ mWh cm}^{-3}$ ),<sup>[51]</sup> NiO//Fe<sub>3</sub>O<sub>4</sub> ( $5.24 \text{ mWh cm}^{-3}$ ),<sup>[52]</sup> Co<sub>3</sub>O<sub>4</sub>//Bi<sub>2</sub>O<sub>3</sub> battery ( $7.74 \text{ mWh cm}^{-3}$ ),<sup>[57]</sup> Zn//NiCo ( $8 \text{ mWh cm}^{-3}$ ),<sup>[55]</sup> and NiO//ZnO battery ( $10.67 \text{ mWh cm}^{-3}$ ).<sup>[45]</sup> Furthermore, a relatively

large energy density of  $4.9 \text{ mWh cm}^{-3}$  is still delivered by our device even at a high power density of  $87.2 \text{ mW cm}^{-3}$ , disclosing its good rate performance. Additionally, as shown in Figure 5b, our quasisolid state Zn//MoO<sub>3</sub> batteries connected in series can power 45 LEDs (3.0 V), showing its great practical value.

### 3. Conclusion

In summary, our studies disclose that the dominant reasons for the electrochemical instability of MoO<sub>3</sub> nanowires are the severe destruction and dissolution of active material. We further demonstrated that the employment of a PVA/ZnCl<sub>2</sub> quasisolid state electrolyte could effectively fix these issues. ZIBs based on the MoO<sub>3</sub> nanowire cathode with quasisolid state electrolyte delivers a decent capacity retention of more than 70.4% after 400 cycles, substantially superior to the one with aqueous electrolyte (27.1%). Moreover, the capacity and energy density of this quasisolid state battery achieve up to  $2.65 \text{ mAh cm}^{-2}$  ( $243.1 \text{ mAh g}^{-1}$ ) at  $0.4 \text{ A g}^{-1}$  and  $14.4 \text{ mWh cm}^{-3}$  at  $9.79 \text{ mW cm}^{-3}$ , respectively, outperforming most of other ZIBs. This work presents the first example of quasisolid state electrolyte stabilized MoO<sub>3</sub> as an ultrahigh capacity cathode material for ZIBs, which will give new insights in the exploration of advanced energy storage systems.

### 4. Experimental Section

**Preparation of MoO<sub>3</sub>:** MoO<sub>3</sub> nanowires were synthesized on carbon cloth through a seed-assisted hydrothermal approach. First, Na<sub>2</sub>MoO<sub>4</sub> · 2H<sub>2</sub>O (2.5 g) was dissolved in the solution containing HCl (5 mL, 37 wt. %) and deionized (DI) water (20 mL). Then, the clean carbon cloth (70 mg) were immersed into the aforesaid solution for 5 min and blow-dried with the help of air blower. Immediately, the dry carbon cloth was further heated in the oven (340 °C) for another 5 min to form MoO<sub>3</sub> nanoparticles on it. The precursor solution was prepared by dissolving (NH<sub>4</sub>)<sub>6</sub>Mo<sub>7</sub>O<sub>24</sub> (0.5 g) in the mixture of concentrated HNO<sub>3</sub> (3 mL, 65 wt. %) and DI water (17 mL). Next, the prepared carbon cloth was immersed into the precursor solution followed by being transferred to a Teflon-lined stainless steel autoclave (25 mL). The autoclave was heated in a drying oven with a heating speed of  $10 \text{ °C min}^{-1}$  to  $140 \text{ °C}$  for 5 min and then cooled down to room temperature. Afterward, the attained carbon cloth were thoroughly washed with DI water and dried, which formed the sample of MoO<sub>3</sub> nanowires. The mass loading of the MoO<sub>3</sub> nanowires deposited on carbon cloth is around  $11.1 \text{ mg cm}^{-2}$  (BT25S, 0.01 mg).

**Fabrication of Quasi Solid State Zn//MoO<sub>3</sub>Battery:** MoO<sub>3</sub>@carbon cloth and zinc plate was assembled together with a separator (NKK separator, Nippon Kodoshi Corporation) between them to form our battery. This PVA/ZnCl<sub>2</sub> gel was made by mixing 2 g polyvinyl alcohol, 10 mL deionized water, and 10 mL 2M ZnCl<sub>2</sub> (5 μL concentrated HCl was added to make ZnCl<sub>2</sub> fully dissolved), and heated at  $85 \text{ °C}$  for 1 h under vigorous stirring. The electrodes and separator were soaked in this gel before assembling. After that, they were piled up layer-by-layer followed by a solidification process to remove excessive water. Finally, the battery was packaged with an area of  $0.5 \text{ cm}^2$  and thickness of  $0.08 \text{ cm}$ .

**UV-Visible Spectroscopy (Dissolution Test):** Standard curve. First, Na<sub>2</sub>MoO<sub>4</sub> · 2H<sub>2</sub>O was dissolved into  $1.84 \text{ mol L}^{-1} \text{ H}_2\text{SO}_4$  to prepare solutions with a Mo concentration of 0, 5, 10, 20, 30,  $50 \text{ μg mL}^{-1}$ . Simultaneously, 100 mL  $250 \text{ g L}^{-1} \text{ KSCN}$ , 100 mL  $50 \text{ g L}^{-1}$  ascorbic acid, 100 mL  $1.84 \text{ mol L}^{-1} \text{ H}_2\text{SO}_4$ , and 5 mL  $0.4 \text{ g L}^{-1} \text{ CuSO}_4$  were mixed together and gently shook to form chromogenic agent. Then, 6 mL of chromogenic agent was added to 5 mL of different concentration of

Mo solutions. Wait for 10 min and then measure absorbance at the wavelength of 470 nm. The value was averaged after three times of parallel experiments. The standard curve was obtained by drawing and fitting Absorbance–C<sub>Mo</sub> curve. Electrolyte sample preparation. 5 mL mixed concentrated H<sub>2</sub>SO<sub>4</sub> and HNO<sub>3</sub> (1:4 for volume ratio) was added to filtered electrolytes. Then, the solutions were heated at  $200 \text{ °C}$  until fully dried. 2 mL mixed concentrated H<sub>2</sub>SO<sub>4</sub> and HNO<sub>3</sub> were added into the dried solution and was heated again. The residue was dissolved by  $1.84 \text{ mol L}^{-1} \text{ H}_2\text{SO}_4$  to make a final volume of 50 mL. The next procedures can be referred to the standard Mo solution test.

**Material Characterization and Electrochemical Measurement:** The morphology, microstructures, and compositions of the electrode materials were analyzed using field-emission SEM (FE-SEM, JSM-6330F), TEM (FEI Tecnai G<sup>2</sup> F30), XPS (ESCALab250, Thermo VG), and XRD (D8 ADVANCE). CV, galvanostatic charge/discharge measurements, GITT, and electrochemical impedance spectroscopy were conducted employing an electrochemical workstation (CHI 760D). The electrochemical performances of Zn//MoO<sub>3</sub> Batteries were tested in a two-electrode system in a 2M ZnCl<sub>2</sub> electrolyte. The dissolution test was conducted on a UV-vis spectrometer (SHIMADZU UV-2600 220 V CH).

### Supporting Information

Supporting Information is available from the Wiley Online Library or from the author.

### Acknowledgements

X.H. and H.Z. contributed equally to this work. The authors acknowledge the financial support of this work received by National Natural Science Foundation of China (21822509, U1810110, and 31530009), Fundamental Research Foundation for Universities of Heilongjiang Province (LGYC2018JQ006), Science and Technology Planning Project of Guangdong Province (2018A050506028), Pearl River Nova Program of Guangzhou (201610010080), Tip-top Scientific and Technical Innovative Youth Talents of Guangdong Special Support Program (2015TQ01C205), and Province key platforms and projects of Guangdong Universities (No. 2017KQNCX195).

### Conflict of Interest

The authors declare no conflict of interest.

### Keywords

cathodes, durability, high-energy, MoO<sub>3</sub>, Zn ion batteries

Received: January 20, 2019

Revised: April 12, 2019

Published online: May 14, 2019

- [1] P. Simon, Y. Gogotsi, B. Dunn, *Science* **2014**, *343*, 1210.
- [2] D. Larcher, J. M. Tarascon, *Nat. Chem.* **2015**, *7*, 19.
- [3] Y. Huang, Y. Zeng, M. Yu, P. Liu, Y. Tong, F. Cheng, X. Lu, *Small Methods* **2018**, *2*, 1700230.
- [4] T. Kou, B. Yao, T. Liu, Y. Li, J. Mater. Chem. A **2017**, *5*, 17151.
- [5] F. Wang, O. Borodin, T. Gao, X. Fan, W. Sun, F. Han, A. Faraone, J. A. Dura, K. Xu, C. Wang, *Nat. Mater.* **2018**, *17*, 543.

- [6] C. Zhu, T. Liu, F. Qian, W. Chen, S. Chandrasekaran, B. Yao, Y. Song, E. B. Duoss, J. D. Kuntz, C. M. Spadaccini, *Nano Today* **2017**, *15*, 107.
- [7] N. Jabeen, A. Hussain, Q. Y. Xia, S. Sun, J. W. Zhu, H. Xia, *Adv. Mater.* **2017**, *29*, 1700804.
- [8] J. Zhou, X. Liu, W. Cai, Y. Zhu, J. Liang, K. Zhang, Y. Lan, Z. Jiang, G. Wang, Y. Qian, *Adv. Mater.* **2017**, *29*, 1700214.
- [9] X. Wang, F. Wang, L. Wang, M. Li, Y. Wang, B. Chen, Y. Zhu, L. Fu, L. Zha, L. Zhang, Y. Wu, W. Huang, *Adv. Mater.* **2016**, *28*, 4904.
- [10] Y. H. Jung, C. H. Lim, J.-H. Kim, D. K. Kim, *RSC Adv.* **2014**, *4*, 9799.
- [11] H. B. Zhao, C. J. Hu, H. W. Cheng, J. H. Fang, Y. P. Xie, W. Y. Fang, T. N. L. Doan, T. K. A. Hoang, J. Q. Xu, P. Chen, *Sci. Rep.* **2016**, *6*, 25809.
- [12] H. Li, C. Han, Y. Huang, Y. Huang, M. Zhu, Z. Pei, Q. Xue, Z. Wang, Z. Liu, Z. Tang, *Energy Environ. Sci.* **2018**, *11*, 941.
- [13] Y. S. Wang, J. Liu, B. J. Lee, R. M. Qiao, Z. Z. Yang, S. Y. Xu, X. Q. Yu, L. Gu, Y. S. Hu, W. L. Yang, K. Kang, H. Li, X. Q. Yang, L. Q. Chen, X. J. Huang, *Nat. Commun.* **2015**, *6*, 6401.
- [14] C. Deng, S. Zhang, Z. Dong, Y. Shang, *Nano Energy* **2014**, *4*, 49.
- [15] C. Xu, B. Li, H. Du, F. Kang, *Angew. Chem., Int. Ed.* **2012**, *51*, 933.
- [16] Y. Zeng, Z. Lin, Y. Meng, Y. Wang, M. Yu, X. Lu, Y. Tong, *Adv. Mater.* **2016**, *28*, 9188.
- [17] N. Zhang, F. Cheng, Y. Liu, Q. Zhao, K. Lei, C. Chen, X. Liu, J. Chen, *J. Am. Chem. Soc.* **2016**, *138*, 12894.
- [18] X. Z. Zhang, H. Li, Y. Zhang, Y. Zeng, Y. Tong, P. Zhang, X. Lu, *Green Energy Environ.* **2018**, *3*, 56.
- [19] Y. Zeng, Y. Meng, Z. Lai, X. Zhang, M. Yu, P. Fang, M. Wu, Y. Tong, X. Lu, *Adv. Mater.* **2017**, *29*, 1702698.
- [20] P. He, M. Yan, G. Zhang, R. Sun, L. Chen, Q. An, L. Mai, *Adv. Energy Mater.* **2017**, *7*, 1601920.
- [21] H. Zhang, R. Wang, D. Lin, Y. Zeng, X. Lu, *ChemNanoMat.* **2018**, *4*, 525.
- [22] M. Yan, P. He, Y. Chen, S. Wang, Q. Wei, K. Zhao, X. Xu, Q. An, Y. Shuang, Y. Shao, *Adv. Mater.* **2018**, *30*, 1703725.
- [23] P. Hu, T. Zhu, X. Wang, X. Wei, M. Yan, J. Li, W. Luo, W. Yang, W. Zhang, L. Zhou, *Nano Lett.* **2018**, *18*, 1758.
- [24] S.-B. Lai, M.-I. Jamesh, X.-C. Wu, Y.-L. Dong, J.-H. Wang, M. Gao, J.-F. Liu, X.-M. Sun, *Rare Met.* **2017**, *36*, 381.
- [25] B. Lee, C. S. Yoon, H. R. Lee, K. Y. Chung, B. W. Cho, S. H. Oh, *Sci. Rep.* **2015**, *4*, 6066.
- [26] C. Yuan, Y. Zhang, Y. Pan, X. Liu, G. Wang, D. Cao, *Electrochim. Acta* **2014**, *116*, 404.
- [27] M. H. Alfaruqi, V. Mathew, J. Gim, S. Kim, J. Song, J. P. Baboo, S. H. Choi, J. Kim, *Chem. Mater.* **2015**, *27*, 3609.
- [28] Y. Zeng, X. Zhang, Y. Meng, M. Yu, J. Yi, Y. Wu, X. Lu, Y. Tong, *Adv. Mater.* **2017**, *29*, 1700274.
- [29] M. S. Chae, J. W. Heo, S.-C. Lim, S.-T. Hong, *Inorg. Chem.* **2016**, *55*, 3294.
- [30] L. Zhang, L. Chen, X. Zhou, Z. Liu, *Adv. Energy Mater.* **2015**, *5*, 1400930.
- [31] D. Kundu, B. D. Adams, V. D. Ort, S. H. Vajargah, L. F. Nazar, *Nat. Energy* **2016**, *1*, 16119.
- [32] J. F. Parker, C. N. Chervin, I. R. Pala, M. Machler, M. F. Burz, J. W. Long, D. R. Rolison, *Science* **2017**, *356*, 415.
- [33] H. L. Pan, Y. Y. Shao, P. F. Yan, Y. W. Cheng, K. S. Han, Z. M. Nie, C. M. Wang, J. H. Yang, X. L. Li, P. Bhattacharya, K. T. Mueller, J. Liu, *Nat. Energy* **2016**, *1*, 16039.
- [34] D. Zheng, H. Feng, X. Zhang, X. He, M. Yu, X. Lu, Y. Tong, *Chem. Commun.* **2017**, *53*, 3929.
- [35] J. Chang, M. Jin, F. Yao, T. H. Kim, V. T. Le, H. Yue, F. Gunes, B. Li, A. Ghosh, S. Xie, Y. H. Lee, *Adv. Funct. Mater.* **2013**, *23*, 5074.
- [36] W. Li, F. Cheng, Z. Tao, J. Chen, *J. Phys. Chem. B* **2006**, *110*, 119.
- [37] A. M. Hashem, H. Groult, A. Mauger, K. Zaghib, C. M. Julien, *J. Power Sources* **2012**, *219*, 126.
- [38] J. Światowska-Mrowiecka, S. de Diesbach, V. Maurice, S. Zanna, L. Klein, E. Briand, I. Vickridge, P. Marcus, *J. Phys. Chem. C* **2008**, *112*, 11050.
- [39] J. O. Besenhard, J. Heydecke, H. P. Fritz, *Solid State Ionics* **1982**, *6*, 215.
- [40] T. Tsumura, M. Inagaki, *Solid State Ionics* **1997**, *104*, 183.
- [41] J. G. Choi, L. T. Thompson, *Appl. Surf. Sci.* **1996**, *93*, 143.
- [42] Y. Xu, Y. Zhu, Y. Liu, C. Wang, *Adv. Energy Mater.* **2013**, *3*, 128.
- [43] X. Fan, Z. Yang, W. Long, Z. Zhao, B. Yang, *Electrochim. Acta* **2013**, *92*, 365.
- [44] W. Sun, F. Wang, S. Hou, C. Yang, X. Fan, Z. Ma, T. Gao, F. Han, R. Hu, M. Zhu, C. Wang, *J. Am. Chem. Soc.* **2017**, *139*, 9775.
- [45] J. Liu, C. Guan, C. Zhou, Z. Fan, Q. Ke, G. Zhang, C. Liu, J. Wang, *Adv. Mater.* **2016**, *28*, 8732.
- [46] H. Wang, Y. Liang, M. Gong, Y. Li, W. Chang, T. Mefford, J. Zhou, J. Wang, T. Regier, F. Wei, *Nat. Commun.* **2012**, *3*, 917.
- [47] N. Zhang, F. Cheng, J. Liu, L. Wang, X. Long, X. Liu, F. Li, J. Chen, *Nat. Commun.* **2017**, *8*, 405.
- [48] X. Wu, Y. Qi, J. J. Hong, Z. Li, A. S. Hernandez, X. Ji, *Angew. Chem.* **2017**, *129*, 13206.
- [49] Z. Guo, Y. Zhao, Y. Ding, X. Dong, L. Chen, J. Cao, C. Wang, Y. Xia, H. Peng, Y. Wang, *Chem* **2017**, *3*, 348.
- [50] Y. Zeng, Z. Lin, Z. Wang, M. Wu, Y. Tong, X. Lu, *Adv. Mater.* **2018**, *30*, 1707290.
- [51] C. Xu, J. Liao, C. Yang, R. Wang, D. Wu, P. Zou, Z. Lin, B. Li, F. Kang, C.-P. Wong, *Nano Energy* **2016**, *30*, 900.
- [52] C. Guan, W. Zhao, Y. Hu, Q. Ke, X. Li, H. Zhang, J. Wang, *Adv. Energy Mater.* **2016**, *6*, 1601034.
- [53] F. Y. Cheng, J. Chen, X. L. Gou, P. W. Shen, *Adv. Mater.* **2005**, *17*, 2753.
- [54] J. Liu, M. Chen, L. Zhang, J. Jiang, J. Yan, Y. Huang, J. Lin, H. J. Fan, Z. X. Shen, *Nano Lett.* **2014**, *14*, 7180.
- [55] Y. Huang, W. S. Ip, Y. Y. Lau, J. Sun, J. Zeng, N. S. S. Yeung, W. S. Ng, H. Li, Z. Pei, Q. Xue, Y. Wang, J. Yu, H. Hu, C. Zhi, *ACS Nano* **2017**, *11*, 8953.
- [56] M.-C. Lin, M. Gong, B. Lu, Y. Wu, D.-Y. Wang, M. Guan, M. Angel, C. Chen, J. Yang, B.-J. Hwang, H. Dai, *Nature* **2015**, *520*, 324.
- [57] R. Liu, L. Ma, G. Niu, X. Li, E. Li, Y. Bai, G. Yuan, *Adv. Funct. Mater.* **2017**, *27*, 1701635.